Science Bulletin 64 (2019) 310–314

Contents lists available at ScienceDirect

Science Bulletin

journal homepage: www.elsevier.com/locate/scib

Science Bulletin
www.scibull.com

Article

Antiferromagnetically ordered Mott insulator and $d + id$ superconductivity in twisted bilayer graphene: a quantum Monte Carlo study

Tongyun Huang, Lufeng Zhang, Tianxing Ma *

Department of Physics, Beijing Normal University, Beijing 100875, China

ARTICLE INFO

Article history:
Received 28 January 2019
Received in revised form 29 January 2019
Accepted 30 January 2019
Available online 21 February 2019

Keywords:
Twisted bilayer graphene
Mott insulator
Superconductivity
Quantum Monte Carlo

ABSTRACT

Using exact quantum Monte Carlo method, we examine the recent novel electronic states seen in magic-angle graphene superlattices. From the Hubbard model on a double-layer honeycomb lattice with a rotation angle $\theta = 1.08^\circ$, we reveal that an antiferromagnetically ordered Mott insulator emerges beyond a critical U_c at half filling, and with a small doping, the pairing with $d + id$ symmetry dominates over other pairings at low temperature. The effective $d + id$ pairing interaction strongly increases as the on-site Coulomb interaction increases, indicating that the superconductivity is driven by electron-electron correlation. Our non-biased numerical results demonstrate that the twisted bilayer graphene shares the similar superconducting mechanism of high temperature superconductors, which is a new and ideal platform for further investigating the strongly correlated phenomena.

1. Introduction

In past decades, studies on the exotic correlated electronic phases in graphene open up a new frontier in condensed matter physics [1–4]. Among these exciting research fields, enormous theoretical proposals have been made on engineering possible novel superconductivity (SC) in graphene [5–19]. Previous studies suggest that it is a very challenging problem to induce SC near the charge neutrality point in graphene as the density of state (DOS) is rather low due to its Dirac-cone band, and if heavily doped, unconventional SC with different pairing symmetry is proposed, while the doping level is beyond current experimental capacity [10–12]. Most recently, a series of breakthrough experiments on magic-angle graphene superlattices have triggered great excitement [20,21]. By arranging two layers of graphenes twisted at a narrow range of particular magic angle, the band structure of such twisted bilayer graphene (TBG) becomes nearly flat, and the Fermi velocity drops to zero in the vicinity of the Fermi energy. Intriguingly, this system is interpreted as a correlated Mott insulator at half filling [20], and when a few extra charge carriers are doped in, the insulator turns into a superconductor at 1.7 K with charge carriers density $\sim 10^{11}$ cm^{-2} [21].

Regarding this ultra low doping density, the transition temperature of 1.7 K is remarkably high, and the SC is suggested to be originated from electron correlation, which has a striking similar trend as that in doped cuprates [22], heavy-fermion [23], iron-based [24] and organic superconductors [25]. Thus, the realization of unconventional SC in TBG provides a relatively simple and more importantly, highly tunable and realistic platform for studying correlated electron physics, especially, which holds promise for several long standing problems, for example, the understanding of unconventional SC, and also may prove to be a significant step in the searching for room-temperature superconductors [20,21]. Moreover, the vicinity between various magnetic orders and SC in high temperature superconductors is one of the most notorious issues. These problems, are the biggest challenge of condensed matter physics [26], and the TBG, may provide an intriguing route to study the largely unknown physics.

However, the nature of the superconducting and the correlated insulating states in TBG are under very active debate [20,21]. Especially, to establish the mechanism and the paring symmetry for the observed SC are among the central theoretical challenges, and different pairing symmetries by various theoretical methods have been proposed [21,27–31]. To win these great challenges, using unbiased numerical techniques is believed to be the only opportunity as Hartree-Fork-type approaches are biased if the electronic correlation dominates in the system. In current work, we aim to identify the Mott physics and the pairing symmetry in TBG by using exact quantum Monte Carlo (QMC) method. Here, our non-biased numerical results almost recover all the novel electronic states seen in TBG where the existence of SC close to an antiferromagnetically

* Corresponding author.
E-mail address: txma@bnu.edu.cn (T. Ma).

https://doi.org/10.1016/j.scib.2019.01.026
2095-9273/

ordered Mott insulator [20,21], which is a hallmark of doped cuprates and other unconventional superconductors [26]. Our study marks the first step in dealing with similar fundamental issues for vertically twist stacked correlated materials, which may open a new direction for the investigation of strongly correlated phases of matter.

2. Model and method

The sketches for TBG with rotation angle $\theta = 1.08^\circ$ and $\theta = 9.43^\circ$ between the layers have been shown in Fig. 1a and b respectively, and θ, which are related to (m,n) by $\cos\theta = \frac{m^2+n^2+4mn}{2(m^2+n^2+mn)}$, coincide with the value of (31,30) and (4,3) for the fully optimized geometries of TBG in Ref. [32]. The parameters (m,n) correspond to the basis vector $\mathbf{v}_1 = m\mathbf{a}_1 + n\mathbf{a}_2$ of the first layer and $\mathbf{v}_2 = n\mathbf{a}_1 + m\mathbf{a}_2$ of the second layer for the non-rotating bilayer graphene, and they merge after one layer rotates the angle θ. Here, $\mathbf{a}_1$ and $\mathbf{a}_2$ are the lattice vectors of each sublattice. In that geometry, each lattice consists of two layers, and each layer includes two interpenetrating triangular sublattices with hexagonal shape such that it preserves most geometric symmetries of graphene [10,12,33]. In each sublattice, the total number of unit cells is $3L^2$ and the total number of lattice sites is $N_s = 2\times 2\times 3L^2$. According to Ref. [32], there is a critical angle $\theta_c = 5^\circ$, and below which the Fermi velocity decreases dramatically toward zero to cause flat bands at the Fermi level. In Fig. 1c, it is clear to see that there is a Van Hove singularity (VHS) around half filling in the DOS calculated from the tight-binding model ($U = 0$) for $N_s = 192$ ($L = 4$) with $\theta = 1.08^\circ$. Our model begins with all of the hoppings in the interlayer, and it includes both the AA and AB-region due to the periodic boundary condition for each layer. Thus, the interplay of those two regions leads to the VHS around the Dirac point, and its behavior is very similar to that calculated on the lattice with $N_s = 11,164$ sites, which is the actual number of atoms in the superlattice unit cell. For comparation, the DOS at $\theta = 9.43^\circ$ is also shown in Fig. 1d, which has a splitting of VHS in higher energy.

Including the electronic correlation, the Hamiltonian for TBG reads [34–36]

$$\begin{aligned} H = & -t\sum_{l\langle i,j\rangle\sigma}\left(a^\dagger_{li\sigma}b_{lj\sigma} + b^\dagger_{li\sigma}a_{lj\sigma}\right) \\ & -\textstyle\sum_{i,j,l\neq l'\sigma} t_{ij}\left(a^\dagger_{li\sigma}a_{l'j\sigma} + a^\dagger_{li\sigma}b_{l'j\sigma} + b^\dagger_{li\sigma}a_{l'j\sigma} + b^\dagger_{li\sigma}b_{l'i\sigma}\right) \\ & +\mu\sum_{i,l,\sigma}\left(a^\dagger_{li\sigma}a_{li\sigma} + b^\dagger_{li\sigma}b_{li\sigma}\right) \\ & +U\sum_{i,l}\left(n_{lai\uparrow}n_{lai\downarrow} + n_{lbi\uparrow}n_{lbi\downarrow}\right), \end{aligned} \tag{1}$$

where $a_{li\sigma}$ ($a^\dagger_{li\sigma}$) annihilates (creates) electrons at site $\mathbf{R}^a_{li}$ of l layer with spin σ (σ=↑, ↓) on sublattice A, $n_{lai\sigma} = a^\dagger_{li\sigma}a_{li\sigma}$, and $b_{li\sigma}$ ($n_{lbi\sigma}$) acts similar but on sublattice B. $t \approx 2.7$eV is the nearest-neighbor (NN) hopping integral, which will be taken as the unit in the following. μ is the chemical potential and U denotes the on-site Hubbard interaction. The interlayer hopping between sites $\mathbf{R}_{1i}$ and $\mathbf{R}_{2j}$ is

$$t_{ij} = t_c e^{-\left[\left(|\mathbf{R}^d_{1i} - \mathbf{R}^{d'}_{2j}|\right) - d_0\right]/\xi}, \tag{2}$$

where $t_c = -0.17, d_0 = 0.335$ nm, and $\xi = 0.0453$ nm [35]. t_{ij} is considered over all sites in the geometry which decreases exponentially with the distance $|\mathbf{R}^d_{1i} - \mathbf{R}^{d'}_{2j}|$, and tends to be zero as the distance is larger than $3.0a$, indicating that the lattice size used in current study is large enough to distinguish the TBG from the monolayer graphene and the normal bilayer graphene. $\mathbf{R}^{d'}_{2j} = \left(\mathbf{R}^d_{2jx}\cos\theta, \mathbf{R}^d_{2jy}\sin\theta\right)$ is the rotated position of $\mathbf{R}^d_{2j}$, and a is the length of carbon-carbon bond. Particularly, t is related to $pp\sigma$ term of Slater-Koster hopping parameters, and t_c is related to $pp\pi$ term.

Our simulations are mostly performed on lattice of $L = 4$ with periodic boundary conditions. To make the finite-size scaling analysis, lattices with $L = 2, 3, 4, 5, 6$ are also simulated. The basic strategy of the finite temperature determinant quantum Monte Carlo (DQMC) method is to express the partition function as a high-dimensional integral over a set of random auxiliary fields. The integral is then accomplished by Monte Carlo techniques. In our simulations, 8,000 sweeps were used to equilibrate the system, and an additional 10,000–200,000 sweeps were then made, each of which generated a measurement. These measurements were split into ten bins which provide the basis of coarse-grain averages and errors were estimated based on standard deviations from the average. In order to assess our results and their accuracy with respect to the infamous sign problem as the particle-hole symmetry is broken, a very careful analysis on the average of sign is illustrated, and results by constrained-path quantum Monte Carlo (CPQMC) method are also presented, where the sign problem is eliminated by the constrained-path approximation [37,38].

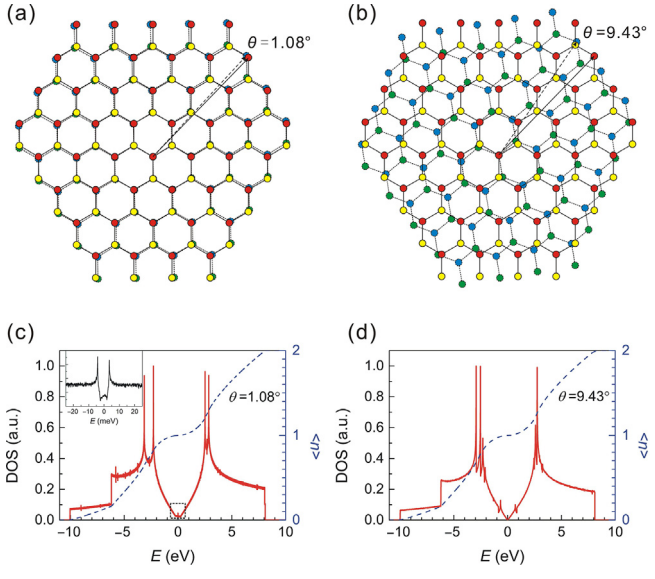

Fig. 1. (Color online) Sketch of TBG with $N_s = 192$ sites is shown for (a) $\theta = 1.08^\circ$ and (b) $\theta = 9.43^\circ$, and not all interlayer hoppings are depicted due to their complex; The DOS is shown for (c) $\theta = 1.08^\circ$ and (d) $\theta = 9.43^\circ$.

3. Results and discussion

As magnetic order plays a key role in the superconducting mechanism of electronic correlated systems, we first study the antiferromagnetic (AFM) spin structure factor

$$S_{\mathrm{AFM}} = \frac{1}{N_s}\left\langle\left[\sum_{lr}\left(\hat{S}^z_{lar} - \hat{S}^z_{lbr}\right)\right]^2\right\rangle, \tag{3}$$

which indicates the onset of long-range AFM order if $\lim_{N_s\to\infty}(S_{\mathrm{AFM}}/N_s) > 0$. Here, $\hat{S}^z_{lar}(\hat{S}^z_{lbr})$ is the z component spin operator on A (B) sublattice of layer l. S_{AFM} for different interactions are calculated on lattices with $L = 2, 3, 4, 5, 6$, and are extrapolated to the thermodynamic limit using polynomial functions in $1/\sqrt{N_s}$. As that shown in Fig. 2a, one can deduce that the critical U_c, where the AFM long range order develops, is around 3.8. Here, we choose $\beta = 12$ as the zero temperature limit. The average sign, $\langle sign\rangle$, with

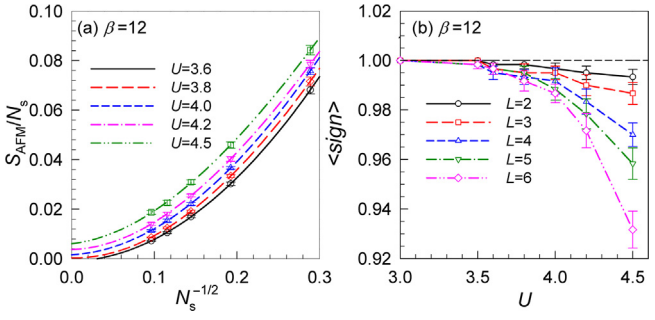

Fig. 2. (Color online) Antiferromagnetic structure factor. (a) Scaling behavior of S_{AFM}/N_s for U at $\beta = 12$. Dash lines are fit of the third-order polynomial in $1/\sqrt{N_s}$. (b) The corresponding $\langle sign\rangle$ at $\beta = 12$.

10,000 runs is shown in Fig. 2b, which is larger than 0.92 at U up to 4.5 and N_s up to 432 for the lowest temperature we reached. In order to obtain the same quality of data as $\langle sign\rangle \simeq 1$, much longer runs are necessary to compensate the fluctuations. Indeed, we can estimate that the runs need to be stretched [39–41] by a factor on the order of $\langle sign\rangle^{-2}$. In our simulations, especially in the following simulation results where the sign problem is much worse, we have increased measurement from 10,000 to 200,000 times to compensate the fluctuations, and thus the results for current parameters are reliable.

One electronic state of high interest is the Mott-like insulator [20], which could be determined by examining the behavior of charge compressibility $\kappa(\mu) = \mathrm{d}\langle n(\mu)\rangle/\mathrm{d}\mu$ at the Fermi level. After analyzing the effect of finite T in the noninteracting limit, we take $\kappa \sim 0.04$ as an appropriate threshold to distinguish between gapped ($\kappa < 0.04$) and gapless ($\kappa > 0.04$) system [42]. Results for $\kappa(\mu)$ evaluated at $\beta = 10$ are depicted in Fig. 3a with various U. Fig. 3a suggests that the system becomes incompressible at $U_c \sim 3.8$, and we can also tell this from Fig. 3b while $\langle n(\mu)\rangle$ converges faster than κ vanishes. Combining results shown in Fig. 2, we identify that the state at half filling with $U > U_c$ is an antiferromagneticlly ordered Mott insulating state. The critical value U_c is slightly smaller than that in monolayer graphene [43], and there

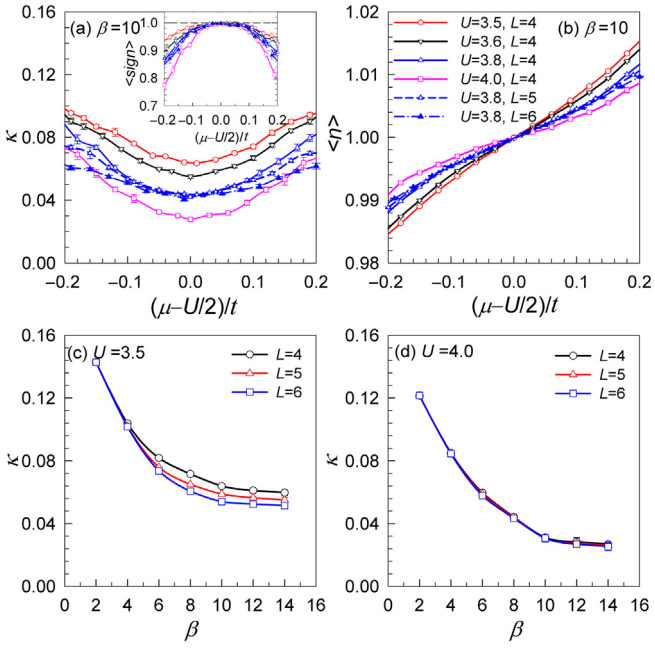

Fig. 3. (Color online) Charge compressibility. (a) κ and (b) $\langle n\rangle$ versus μ at $\beta = 10$ for several interaction strengths. The dependence of L for κ at (c) $U = 3.5$ and (d) $U = 4.0$. Inset: the corresponding $\langle sign\rangle$ for different U and L at $\beta = 10$.

is no potential for spin liquid phase in magic TBG. The $\langle sign\rangle$ shown in the insert of Fig. 3a, is mostly larger than 0.75 for κ at $\beta = 10$ with $L = 4, 5, 6$ and $U \leqslant 4.0$. We further consider the finite lattice sizes effect on κ and $\langle n\rangle$ in the metallic and insulating region, respectively. Our calculations show that, in the metallic region, Fig. 3c, it shows a stronger size dependence, while in the insulating region, Fig. 3d, it is nearly free of finite size effect.

To investigate the superconducting property of TBG, we compute the pairing susceptibility

$$P_\alpha = \frac{1}{N_s}\sum_{l,ij}\int_0^\beta \mathrm{d}\tau\langle\Delta_{l\alpha}^\dagger(i,\tau)\Delta_{l\alpha}(j,0)\rangle, \tag{4}$$

where α stands for the pairing symmetry. Due to the constraint of on-site Hubbard interaction in Eq. (1), pairing between two sublattices is favored and the corresponding order parameter

$$\Delta_{l\alpha}^\dagger(i) = \sum_{\mathbf{l}} f_\alpha^\dagger(\delta_{\mathbf{l}})\left(a_{li\uparrow}b_{li+\delta_{\mathbf{l}}\downarrow} - a_{li\downarrow}b_{li+\delta_{\mathbf{l}}\uparrow}\right)^\dagger, \tag{5}$$

with $f_\alpha(\boldsymbol{\delta}_{\mathbf{l}})$ being the form factor of pairing function. In order to extract the intrinsic pairing interaction in finite system, one should subtract from P_α its uncorrelated single-particle contribution $\widetilde{P}_\alpha$, which is achieved by replacing $\left\langle a_{li\downarrow}^\dagger a_{lj\downarrow} b_{i+\delta_{\mathbf{l}}\uparrow}^\dagger b_{j+\delta_{\mathbf{l}'}\uparrow}\right\rangle$ in Eq. (5) with $\left\langle a_{i\downarrow}^\dagger a_{j\downarrow}\right\rangle\left\langle b_{i+\delta_{\mathbf{l}}\uparrow}^\dagger b_{j+\delta_{\mathbf{l}'}\uparrow}\right\rangle$, and we have the intrinsic pairing interaction $\mathbf{P}_\alpha = P_\alpha - \widetilde{P}_\alpha$.

In Eq. (5), the vectors $\delta_{\mathbf{l}}$ ($\mathbf{l} = 1, 2, 3$) denote the NN inter sublattice connections sketched in Fig. 4. Considering the special structure of honeycomb lattice, the possible pairing symmetries are given by (a) extended S (ES) (b) $d + id$ and (c) $p + ip$ wave [10,12,44]. These different pairing symmetries are distinguished by different phase shifts upon $\pi/3$ or $2\pi/3$ rotations. The singlet ES wave and NN-bond $d + id$ pairing has the form factor

$$f_{ES}(\delta_{\mathbf{l}}) = 1, \quad \mathbf{l} = 1, 2, 3, \tag{6}$$

$$f_{d+id}(\delta_{\mathbf{l}}) = \mathrm{e}^{\mathrm{i}(\mathbf{l}-1)\frac{2\pi}{3}}, \quad \mathbf{l} = 1, 2, 3, \tag{7}$$

for whatever sublattice A and B, while the NN-bond f_{p+ip} is different for A and B sublattice, where

$$f_{p+ip}(\delta_{\mathbf{al}}) = \mathrm{e}^{\mathrm{i}(\mathbf{l}-1)\frac{2\pi}{3}}, \quad \mathbf{l} = 1, 2, 3, \tag{8}$$

for A, and accordingly the phase on the same link for B, there is a π phase shift, $f_{p+ip}(\delta_{\mathbf{bl}}) = \mathrm{e}^{\mathrm{i}\left[(\mathbf{l}-1)\frac{2\pi}{3}+\pi\right]}$. We also studied longer range pairings by adding next nearest neighbour (NNN) bond pairing for $d + id$ wave symmetry, which have the following form factors

$$f_{d+id}(\delta_{\mathbf{l}}) = \mathrm{e}^{\mathrm{i}(\mathbf{l}-1)\frac{2\pi}{3}} \quad \mathbf{l} = 1, 2, 3 \ldots 6. \tag{9}$$

As it is expected that fermion systems with strong on-site repulsion may exhibit SC induced by AFM spin fluctuations, and from the behavior of magnetic correlation shown in Fig. 2, it seems that the pair formation is possible through a similar mechanism in

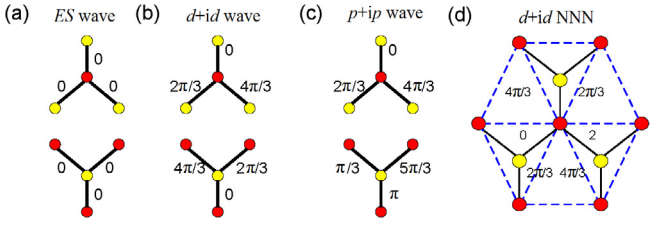

Fig. 4. (Color online) Phases of the pairing symmetries of (a) ES (b) $d + id$ (c) $p + ip$ and (d) $d + id$ wave with next nearest neighbour.

TBG. In the following, we discuss the behavior of the effective pairing interaction in a very low doped region, which is what the experiment has been performed [21].

Fig. 5 shows the temperature dependent $\mathbf{P}_\alpha$ for different pairing symmetries at (a) $\langle n\rangle = 0.97$ and (b) $\langle n\rangle = 0.95$ with $U = 3.0$. It is clearly to see that, the effective pairing interaction with $d + id$ symmetry is always positive and increases with the lowering of temperature, and it is almost independent on lattice size in high temperature region, and the dependence on lattice size is very weak in low temperature region. Such a temperature dependence of $\mathbf{P}_{d+id}$ suggests effective attractions generated between electrons and the instability toward SC in the system at low temperatures for both $\langle n\rangle = 0.97$ and $\langle n\rangle = 0.95$. As for the other two pairing symmetries, $p + ip$ wave and $d + id$ NNN shown, our DQMC results yield negative effective pairing interactions, reflecting the fact that the realization of the $d + id$ symmetry at low temperatures will suppress other competing pairing channels.

Moreover, Fig. 6a and b show that $\mathbf{P}_{d+id}$ enhances with larger U. Especially, $\mathbf{P}_{d+id}$ tends to diverge in low temperature region as $U > 3.0$, and the increasing U tends to promote such diverge. This demonstrates that the $d + id$ pairing SC is driven by strong electronic correlation, which is different from those that electronic correlation suppresses the $d + id$ pairing SC in single layer graphene [10]. In addition, the sign problem only tends to be worse for $U = 4.0$ as $\beta > 8.0$, while which is not important as the dominant pairing symmetry is robust on the temperature.

In general, to determine which pairing symmetry is dominant by numerical calculation for finite size models, we had better to look at the long-range part of the ground state pair-correlation function [10,38,45], which could be achieved by the CPQMC method. In Fig. 7a, the distance dependent pairing-pairing correlation at zero temperature, $C_\alpha(r) = \Sigma_l\langle\Delta^\dagger_{l\alpha}(i)\Delta_{l\alpha}(j)\rangle$,is shown for $\langle n\rangle = 145/150 \simeq 0.97$. It is clear to see that the $C_{d+id}(r)$ is larger than $C_{ES}(r)$ and $C_{p+ip}(r)$ for all long-range distances between electron pairs. This reenforces our finding that the $d + id$ pairing symmetry dominates other pairing symmetries. We also examined the vertex contributions $\mathbf{V}_\alpha = C_\alpha - \widetilde{C}_\alpha$ in Fig. 7b, which increase as the interactions increase, indicating the importance of electronic correlation in enhancing SC.

4. Summary

In summary, we study the spin correlation, the charge compressibility and the superconducting pairing symmetry in TBG by using exact QMC method. From a double-layer honeycomb lattice with a rotation angle $\theta = 1.08^\circ$, we almost recover all the recent experimentally observed novel electronic states in TBG. At half filling, an antiferromagnetically ordered Mott insulator emerges beyond a critical $U_c \sim 3.8$. With a finite doping, the pairing with $d + id$ symmetry dominates over other pairing symmetries, and it increases fast as the interaction increases, indicating that the SC is driven by strong electronic correlations. Our exact numerical results demonstrate that the TBG holds a very similar interaction driven phase diagram of doped cuprates and other high temperature superconductors, which may provide a new and ideal platform to the unified understanding of the superconducting mechanism in electronic correlated system. Moreover, our results are obtained with a system of original geometry which is smaller than the actual Moiré unit cell by one order of magnitude. To justify that our simulation does capture the true physics of magic TBG, we also compare our results with the simulation on one effective model [46], and it is highly significant to see that the simulation on the effective model agrees with our data on the original geometry. This might be even more interesting, which may open a new perspective regarding applications of QMC which might interest an even broader community.

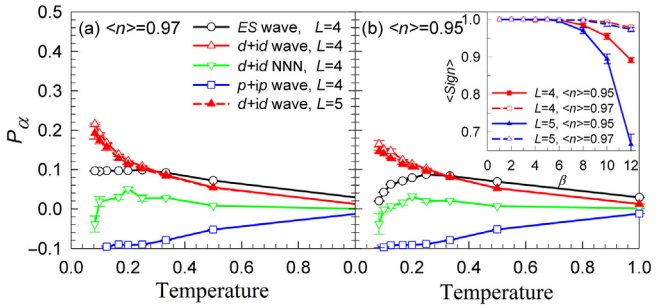

Fig. 5. (Color online) $\mathbf{P}_\alpha$ as a function of temperature at (a) $\langle n\rangle = 0.97$ and (b) $\langle n\rangle = 0.95$ for $U = 3.0$. Inset: the temperature-dependent $\langle sign\rangle$ at $\langle n\rangle = 0.95, 0.97$ with the corresponding L for $U = 3.0$.

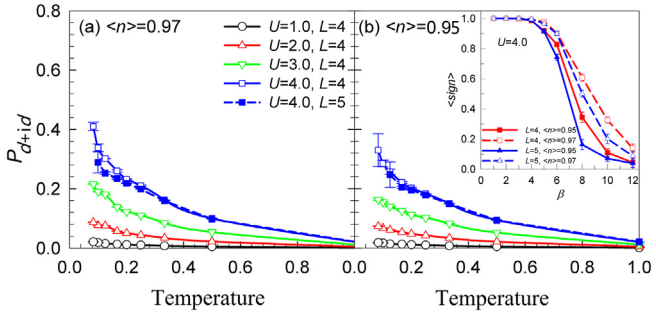

Fig. 6. (Color online) $\mathbf{P}_{d+id}$ as a function of temperature at (a) $\langle n\rangle = 0.97$ and (b) $\langle n\rangle = 0.95$ with different U. Inset: the temperature-dependent $\langle sign\rangle$ at $\langle n\rangle = 0.95, 0.97$ with the corresponding L for $U = 4.0$.

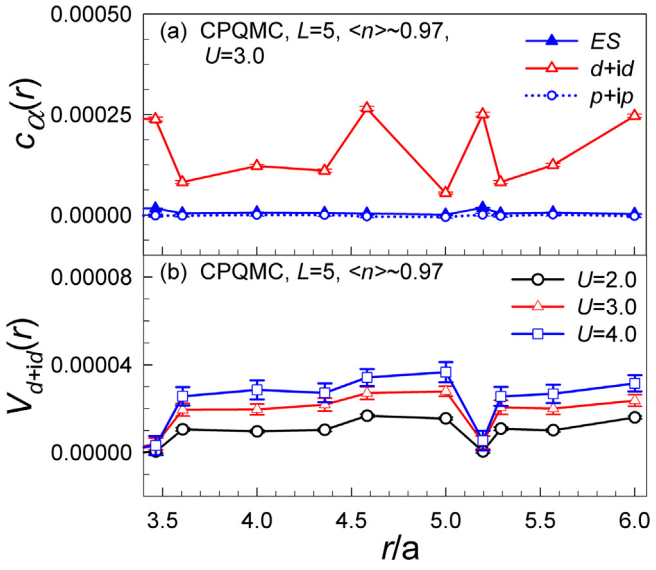

Fig. 7. (Color online) C_α as a function of r for (a) different pairing symmetries with $U = 3.0$, (b) the vertex contributions of $d + id$-wave with different U at $\langle n\rangle \simeq 0.97$ and $L = 5$.

Conflict of interest

The authors declare that they have no conflict of interest.

Acknowledgments

This work was supported by the National Natural Science Foundation of China (11374034 and 11334012), and Beijing Natural

Science Foundation (1192011). We acknowledge the support of HSCC of Beijing Normal University, and phase 2 of the Special Program for Applied Research on Super Computation of the NSFC-Guangdong Joint Fund.

Author contributions

T. Huang and L. Zhang performed the simulations and analyses and prepared the figures; T. Ma directed the investigation and wrote the paper. The manuscript reflects the contributions of all authors.

References

[1] Novoselov KS, Geim AK, Morozov SV, et al. Two-dimensional gas of massless Dirac fermions in graphene. Nature 2005;438:197–200.
[2] Zhang Y, Tan Y-W, Stormer HL, et al. Experimental observation of the quantum hall effect and Berry's phase in graphene. Nature 2005;438:201–4.
[3] Peres NMR. Colloquium: the transport properties of graphene: an introduction. Rev Mod Phys 2010;82:2673–700.
[4] Das Sarma S, Adam S, Hwang EH, et al. Electronic transport in two-dimensional graphene. Rev Mod Phys 2011;83:407–70.
[5] Baskaran G. Resonating-valence-bond contribution to superconductivity in MgB_2. Phys Rev B 2002;65:212505.
[6] Black-Schaffer AM, Doniach S. Resonating valence bonds and mean-field d-wave superconductivity in graphite. Phys Rev B 2007;75:134512.
[7] Pathak S, Shenoy VB, Baskaran G. Possible high-temperature superconducting state with a *d+id* pairing symmetry in doped graphene. Phys Rev B 2010;81:085431.
[8] Uchoa B, Castro Neto AH. Superconducting states of pure and doped graphene. Phys Rev Lett 2007;98:146801.
[9] Kopnin NB, Sonin EB. BCS superconductivity of Dirac electrons in graphene layers. Phys Rev Lett 2008;100:246808.
[10] Ma T, Huang Z, Hu F, et al. Pairing in graphene: a quantum Monte Carlo study. Phys Rev B 2011;84:121410.
[11] Nandkishore R, Levitov LS, Chubukov AV. Chiral superconductivity from repulsive interactions in doped graphene. Nat Phys 2012;8:158–63.
[12] Ma T, Yang F, Yao H, et al. Possible triplet *p+ip* superconductivity in graphene at low filling. Phys Rev B 2014;90:245114.
[13] Nandkishore R, Thomale R, Chubukov AV. Superconductivity from weak repulsion in hexagonal lattice systems. Phys Rev B 2014;89:144501.
[14] Raghu S, Kivelson SA, Scalapino DJ. Superconductivity in the repulsive Hubbard model: an asymptotically exact weak-coupling solution. Phys Rev B 2010;81:224505.
[15] Qi X-L, Zhang S-C. Topological insulators and superconductors. Rev Mod Phys 2011;83:1057–110.
[16] Hasan MZ, Kane CL. Colloquium: topological insulators. Rev Mod Phys 2010;82:3045–67.
[17] Hosseini MV, Zareyan M. Model of an exotic chiral superconducting phase in a graphene bilayer. Phys Rev Lett 2012;108:147001.
[18] Profeta G, Calandra M, Mauri F. Phonon-mediated superconductivity in graphene by lithium deposition. Nat Phys 2012;8:131–4.
[19] Levitov LS, Chubukov AV. Chiral superconductivity from repulsive interactions in doped graphene. Nat Phys 2012;8:158–63.
[20] Cao Y, Fatemi V, Demir A, et al. Correlated insulator behaviour at half-filling in magic-angle graphene superlattices. Nature 2018;556:80–4.
[21] Cao Y, Fatemi V, Fang S, et al. Unconventional superconductivity in magic-angle graphene superlattices. Nature 2018;556:43–50.
[22] Bednorz JG, Müller KA. Possible high T_c superconductivity in the Ba-La-Cu-O system. Z Phys B 1986;64:189–93.
[23] Steglich F, Aarts J, Bredl CD, et al. Superconductivity in the presence of strong Pauli paramagnetism: $CeCu_2Si_2$. Phys Rev Lett 1979;43:1892–6.
[24] Kamihara Y, Watanabe T, Hirano M, et al. Iron-based layered superconductor LaFeAs ($x = 0.05 - 0.12$) with T_c = 26 K. J Am Chem Soc 2008;130:3296–7.
[25] Jerome D, Mazaud A, Ribault M, et al. Superconductivity in a synthetic organic conductor (TMTSF)2PF6. J Phys Lett 1980;41:95–8.
[26] Scalapino DJ. A common thread: the pairing interaction for unconventional superconductors. Rev Mod Phys 2012;84:1383–417.
[27] Xu C, Balents L. Topological superconductivity in twisted multilayer graphene. Phys Rev Lett 2018;121:087001.
[28] Roy B, Juricic V. Unconventional superconductivity in nearly flat bands in twisted bilayer graphene. arXiv:1803.11190.
[29] Baskaran G. Theory of emergent josephson lattice in neutral twisted bilayer graphene (moiŕe is different). arXiv:1804.00627.
[30] Dodaro JF, Kivelson SA, Schattner Y, et al. Phases of a phenomenological model of twisted bilayer graphene. Phys Rev B 2018;98:075154.
[31] Ramires A, Lado JL. Electrically tunable gauge fields in tiny-angle twisted bilayer graphene. Phys Rev Lett 2018;121:146801.
[32] Uchida K, Furuya S, Iwata J-I, et al. Atomic corrugation and electron localization due to Moiré patterns in twisted bilayer graphenes. Phys Rev B 2014;90:155451.
[33] Ma T, Hu F, Huang Z, et al. Controllability of ferromagnetism in graphene. Appl Phys Lett 2010;97:112504.
[34] Lopes dos Santos JMB, Peres NMR, Castro Neto AH. Graphene bilayer with a twist: electronic structure. Phys Rev Lett 2007;99:256802.
[35] Li S-Y, Liu K-Q, Yin L-J, et al. Splitting of Van Hove singularities in slightly twisted bilayer graphene. Phys Rev B 2017;96:155416.
[36] Suárez Morell E, Correa JD, Vargas P, et al. Flat bands in slightly twisted bilayer graphene: tight-binding calculations. Phys Rev B 2010;82:121407.
[37] Zhang S, Carlson J, Gubernatis JE. Constrained path quantum Monte Carlo method for Fermion ground states. Phys Rev Lett 1995;74:3652–5.
[38] Zhang S, Carlson J, Gubernatis JE. Pairing correlations in the two-dimensional Hubbard model. Phys Rev Lett 1997;78:4486–9.
[39] Blankenbecler R, Scalapino DJ, Sugar RL. Monte Carlo calculations of coupled boson-fermion systems. I. Phys Rev D 1981;24:2278–86.
[40] Santos RRd. Introduction to quantum Monte Carlo simulations for fermionic systems. Braz J Phys 2003;33:36–54.
[41] Yang G, Xu S, Zhang W, et al. Room-temperature magnetism on the zigzag edges of phosphorene nanoribbons. Phys Rev B 2016;94:075106.
[42] Ma T, Zhang L, Chang C-C, et al. Localization of interacting Dirac Fermions. Phys Rev Lett 2018;120:116601.
[43] Sorella S, Otsuka Y, Yunoki S. Absence of a spin liquid phase in the Hubbard model on the honeycomb lattice. Sci Rep 2012;2:992.
[44] Ma T, Lin H-Q, Gubernatis JE. Triplet $p + ip$ pairing correlations in the doped Kane-Mele-Hubbard model: a quantum Monte Carlo study. Europhys Lett 2015;111:47003.
[45] Dagotto E, Riera J. Indications of $d_{x^2-y^2}$ superconductivity in the two dimensional $t - j$ model. Phys Rev Lett 1993;70:682–5.
[46] Yuan NFQ, Fu L. Model for the metal-insulator transition in graphene superlattices and beyond. Phys Rev B 2018;98:045103, (E) Phys Rev B 2018;98:079901.

Tongyun Huang received his M. S. degree in Capital Normal University, and he is pursuing his Doctoral degree in Beijing Normal University currently. His research interest focuses on unconventional superconductors and topologic properties in two dimensional strongly correlated system.

Tianxing Ma is a Professor of Department of Physics, Beijing Normal University. He is working in the field of condensed matter physics theory. His research interest includes development of numerical method for electronic correlated system, and study on the competition between magnetism and superconductivity, the superconducting mechanism of unconventional superconductors, as well as the phase transition and novel quantum states in strongly correlated electronic systems.